


## Sixth-Order Degenerate Band Edge in Coupled Microstrip Waveguides

Farshad Yazdi<sup>1</sup>, Dmitry Oshmarin<sup>1</sup>, Tarek Mealy<sup>1</sup>, Ahmad T. Almutawa<sup>1</sup>, Alireza Nikzamir<sup>1</sup>, and Filippo Capolino<sup>1\*</sup>

*Department of Electrical Engineering and Computer Science, University of California, Irvine, California 92697, USA*

 (Received 3 November 2021; revised 21 March 2022; accepted 26 April 2022; published 27 June 2022)

We show the physical realization and experimental demonstration of an exceptional point of sixth-order degeneracy in a triple-ladder (or three-way) microwave waveguide realized using three coupled microstrips on a grounded dielectric substrate. This three-way waveguide supports six Bloch eigenmodes, and all coalesce into a degenerate single eigenmode at a given frequency. The three-way waveguide is gainless, and this exceptional point is associated with a vanishing-group velocity and its multiple derivatives. Indeed, the  $\omega - k$  dispersion diagram that we call the sixth-order degenerate band edge (6DBE) has six coalescing branches. We provide experimental verification of a sixth-order exceptional point by evaluating the degenerate wave number–frequency–dispersion diagram from the measurement of scattering parameters of a six-port unit cell. We also show the resonant behavior of a cavity made of the three-way waveguide with finite length. The unique properties of 6DBE can be exploited to design innovative high- $Q$  resonators, oscillators, filters, and pulse-shaping devices.

DOI: [10.1103/PhysRevApplied.17.064049](https://doi.org/10.1103/PhysRevApplied.17.064049)

Sixth-order degeneracy in electromagnetic waveguides means that six eigenmodes coalesce and form a single degenerate mode. Here, we imply that the degeneracy is in both *wave numbers* and *polarization states* of the six Bloch eigenmodes in a waveguide, forming a sixth-order degenerate band edge (6DBE).

The concept of the degeneracy of the eigenvalues and eigenvector was discussed in Refs. [1–4]. A particular class of exceptional points of degeneracy (EPD) in periodic structures is known as a degenerate band edge (DBE), where *four* eigenmodes in a periodic passive lossless waveguide coincide at the band edge [5–10]. Notably, the presence of the DBE and the 6DBE, discussed here, do not require the presence of losses and gain in the system. The fourth-order DBE is shown in periodic layered media [5], periodic transmission lines [11,12], and metallic [7] and optical waveguides [13–15]. An experimental demonstration of the DBE was shown in microstrip technology [9,16], a circular metallic waveguide [17], and an optical waveguide [14]. A strong resonance was shown experimentally in Ref. [18] using a variation of the DBE, called the split band edge. In Ref. [11], a double-ladder periodic microstrip waveguide was introduced that exhibited a DBE, and in Ref. [9], it was shown that such a structure exhibited a higher quality factor and stability advantages associated with DBE resonance. In Ref. [19], implementation of a three-way partially coupled microstrip

waveguide using lumped elements was presented, demonstrating a stationary inflection point (SIP) associated with a real wave number, which was a special EPD of third order realizable in lossless waveguides. The experimental demonstration of the SIP was shown in Ref. [20].

Here, we demonstrate theoretically and experimentally the existence of a 6DBE in the Bloch-wave-number–frequency–dispersion relation for a periodic waveguide implemented by three coupled microstrip lines, as in Fig. 1. This condition happens when six Floquet-Bloch modes (eigenstates) coincide at the center or at the boundary of the Brillouin zone; here, the intended wave-number interval is  $(0, 2\pi/d)$ , where  $d$  is the period of the waveguide. At the 6DBE, the modal Floquet-Bloch dispersion is characterized by  $(\omega_d - \omega) \propto (k - k_d)^6$ , where  $k$  is the Floquet-Bloch wave number,  $\omega$  is the angular frequency—in this paper, the 6DBE wave number is at  $k_d = \pi/d$  (at the center of the Brillouin zone)—and  $\omega_d$  is the angular frequency at which the 6DBE occurs. The exponent 6 indicates the sixth-order degeneracy, implying that not only the group velocity,  $v_g = \partial\omega/\partial k$ , of the Floquet-Bloch mode vanishes at the 6DBE, but also  $\partial^n\omega/\partial k^n = 0$  for  $n = 1-5$ , while  $\partial^6\omega/\partial k^6 \neq 0$ .

The proposed 6DBE has a band stop, as illustrated in Fig. 1(b), which results in high-quality resonance behavior, as we discuss later. This makes the 6DBE beneficial for applications that require high  $Q$ , such as oscillators. The 6DBE has a flatter dispersion than that of lower EPD orders, where the dispersion relation is a function of order  $N$ , as  $(\omega - \omega_e) \propto (k - k_e)^N$ , like the DBE (which has

\*f.capolino@uci.edu

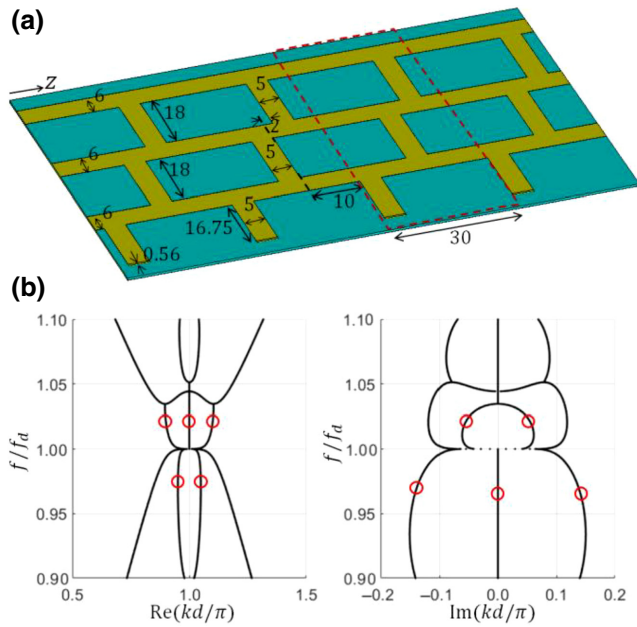


FIG. 1. (a) Periodic “three-way” waveguide, made of three coupled microstrip lines over a grounded dielectric substrate that exhibits a sixth-order DBE. Grounded substrate has a dielectric constant of three, and the stubs are short circuited at their end. (b) Wave-number–frequency–dispersion diagram of the six Floquet–Bloch eigenmodes in the periodic three-way waveguide, showing the 6DBE frequency at  $f_d = 2.95$  GHz, where six dispersion curves coalesce at a single point with wave number  $k_d = \pi/d$ . Branches that represent two modes are denoted by a red circle. When losses are considered, the dispersion diagram is modified and shown later in Fig. 3.

$N = 4$ ) and the SIP (which has  $N = 3$ ). Therefore, the proposed waveguide that exhibits the 6DBE tends to have a higher quality factor than that of others with a lower-order EPD and the same length. The presence of perturbations limits  $Q$ , which is difficult to quantify in general terms when we compare the EPDs of various orders (see Ref. [15] for a study on how perturbations affect  $Q$ ).

We provide a simple implementation of the 6DBE in a three-way waveguide made of three coupled microstrips over a grounded dielectric substrate (Fig. 1). The unit cell of the three-way microstrip is a six-port network that is an extension of the four-port unit-cell circuit of lumped elements in Ref. [21] and of the four-port unit-cell microstrip line in Ref. [9]. Implementation in other waveguide technologies involving a three-way structure (i.e., three coupled waveguides) is possible as well. Notably, in general terms of idealized propagation based on coupled-mode theory, a sixth-order degeneracy was discussed in Ref. [13]. Furthermore, the 6DBE was already shown via transmission-line (TL) simulations in a coupled-resonator optical waveguide, together with a possible application as a low-threshold laser [22]. This paper provides an experimental demonstration of the occurrence of the 6DBE

in a waveguide at microwave frequencies and shows the resonance behavior in a cavity made of a finite-length structure.

To obtain a 6DBE in *reciprocal* waveguide structures, a coupling between at least three modes, for example, in the three microstrip waveguides shown in Fig. 1, is required. This waveguide allows six modes to exist; three modes in each direction. The six modes coalesce into a single eigenmode at the 6DBE frequency,  $\omega_d$ , by resorting to proper coupling and symmetry breaking in the three periodic waveguides. In Fig. 1(a), the proposed unit cell of such a three-way periodic waveguide is shown with a red dashed line. The structure has a period of  $d = 30$  mm. For its characterization, we define six microstrip electromagnetic “ports.” We consider first a lossless structure made of microstrip coupled transmission lines that are implemented on a grounded dielectric substrate with a thickness of 0.508 mm (20 mil), and a dielectric constant of 3.

To analyze and calculate the eigenmodes of the periodic waveguide, we use a transfer-matrix formalism, which is discussed in detail in Refs. [23,24]. We define a six-dimensional state vector,  $\Psi(z) = [\mathbf{V}^T(z), \mathbf{I}^T(z)]^T$ , to describe the evolution of the eigenmodes, where  $T$  denotes the transpose operation;  $\mathbf{V}(z) = [V_1, V_2, V_3]^T$  and  $\mathbf{I}(z) = [I_1, I_2, I_3]^T$  are the vectors that represent the voltage (referred to the ground) and current, respectively, in each of the three microstrips [25]. The evolution of this state vector from a coordinate  $z_1$  to  $z_2$  is then described by  $\Psi(z_2) = \mathbf{T}(z_2, z_1)\Psi(z_1)$ , in which  $\mathbf{T}$  is the  $6 \times 6$  transfer matrix [23]. The results shown in Fig. 1(b) are calculated based the transfer matrix,  $\mathbf{T}$ , that is obtained from circuit simulation, where we simulate one unit cell by cascading several microstrip-equation-based blocks. Full-wave simulations are instead used to generate the results shown in Figs. 2 and 3 where the transfer matrix,  $\mathbf{T}$ , is obtained by transforming the  $6 \times 6$  S-parameter matrix for the six-port unit cell into a transfer matrix. The six Floquet–Bloch eigenmodes in the periodic three-way waveguide satisfy  $\Psi(z + d) = e^{-jkd}\Psi(z)$ , where  $d$  is the length of the unit cell shown in Fig. 1(a), and we implicitly assume the time convention  $\exp(j\omega t)$ . The six wave numbers are obtained by solving the eigenvalue problem:

$$\mathbf{T}\Psi(z) = e^{-jkd}\Psi(z), \quad (1)$$

the eigenvalues of which are calculated from

$$\det[\mathbf{T}(z + d, z) - e^{-jkd}\mathbf{1}] = 0, \quad (2)$$

where  $\mathbf{1}$  is the  $6 \times 6$  identity matrix.

The coalescence parameter that defines the closeness to the 6DBE is given by

$$C = \frac{1}{15} \sum_{\substack{m=1, n=1 \\ m \neq n}}^6 |\sin(\theta_{mn})|, \quad \cos(\theta_{mn}) = \frac{|(\Psi_m, \Psi_n)|}{\|\Psi_m\| \|\Psi_n\|}, \quad (3)$$

where  $\theta_{mn}$  represents the angle between two eigenvectors  $\Psi_m$  and  $\Psi_n$  in a six-dimensional complex vector space calculated from Eq. (1), with norms  $\|\Psi_m\|$  and  $\|\Psi_n\|$  and  $(\Psi_m, \Psi_n)$  as their inner product (involving complex conjugation). This coalescence parameter helps to determine the closeness of a system to having a 6DBE and distinguishing this 6DBE from other EPDs with different orders (like the regular band edge or the DBE). The 6DBE is found by tuning the dimensions of the unit cell to minimize the six-eigenvector coalescence parameter in Eq. (3), where the eigenvectors are calculated from the eigenvalue problem in Eq. (1). The optimized dimensions are shown in Fig. 1(a).

The dispersion diagram, which is the relationship between frequency and the complex-valued Bloch wave numbers, in a lossless and infinitely long periodic waveguide, is depicted in Fig. 1(b) and is calculated based on a microstrip-waveguide transmission-line model using the circuit simulator implemented in the advanced design system by Keysight. The dispersion diagram is obtained by evaluating the eigenvalues  $e^{-jkd}$  derived from the transfer matrix of the three-way waveguide unit cell at each frequency and then converting them into Floquet-Bloch wave numbers. At the 6DBE frequency of 2.95 GHz, one observes that six curves coalesce. We use red circles in Fig. 1(b) to show overlapping branches in either the real or imaginary parts of the wave numbers. At the 6DBE, the dispersion relationship is locally characterized as  $(\omega_d - \omega) \approx h(k - k_d)^6$ , where  $h$  is a parameter that defines the flatness of the dispersion near the degeneracy frequency,  $f_d = \omega_d/(2\pi) = 2.95$  GHz. Based on the real and imaginary branches of the dispersion diagram shown in Fig. 1(b), no mode can propagate in a frequency range just above  $\omega_d$  because of a band gap [indeed,  $\text{Im}(k) \neq 0$  for all six modes]. In the range  $0.9f_d < f < f_d$ , only two modes can propagate (one in each  $z$  direction), and the other four modes are evanescent, since they have  $\text{Im}(k/k_d) \neq 0$ ; below  $f = 0.9f_d$ , other cutoff conditions occur but are not discussed in this paper, since they do not exhibit a sixth-order degeneracy. In the three-way waveguide in Fig. 1(a), when working at a frequency near the 6DBE frequency, interesting features are observed, such as “giant” resonance, enhanced quality factor, and the unique energy distribution inside the 6DBE cavity, in analogy to what is observed in waveguides with a fourth-order DBE [5,8,24,25].

The 6DBE condition is manifested when the transfer matrix is “defective,” and a complete basis of eigenvectors

cannot be found [3,26]. The 6DBE is obtained by properly choosing the coupling between the three coupled waveguides (TLs), and it can be shown that the six independent eigenvectors coalesce into a single degenerate eigenvector. This degeneracy occurs if, and only if, the transfer matrix is similar to a Jordan canonical matrix form, as discussed in Refs. [9,15]. The coalescence of the six eigenvectors can be demonstrated using the coalescence parameter concept introduced in Ref. [9] for a fourth-order degeneracy and is discussed next for the 6DBE, showing that the distance between the six eigenvectors decreases to a minimum value that depends on the amount of losses and tolerances in the system.

We observe the resonance of the passive waveguide made of a finite number of cascaded unit cells shown in Fig. 1(a). The full-wave analysis here accounts for all losses in the dielectric, conductor, and radiation losses. We use the same substrate as that considered to generate the results in Fig. 1(b) but now include losses, i.e., with a loss tangent of  $\tan \delta = \epsilon''/\epsilon' = 0.001$  (Rogers RO3003), with conductors (microstrip and ground plane) that are made of copper with a thickness of  $35 \mu\text{m}$  and a conductivity of  $5.8 \times 10^7$  S/m. A resonator made of a finite-length waveguide with unit cells as in Fig. 1(a) exhibits its resonance, called the 6DBE resonance, at a frequency close to  $f_d$ . Such a resonance exhibits some interesting and unique properties, as shown in Ref. [8], such as a high quality factor and its scaling with the resonator length and the distinctive energy distribution inside the finite-length cavity, which are beneficial in oscillator, sensing, and pulse-shaping applications [24,27,28].

We study the resonance behavior by constructing a finite structure made of eight unit cells as shown in Fig. 2(a), with all terminals connected to a short circuit, except the middle TL at the structure’s left end. We assume an phasor voltage of 1 V at the input of the resonator and observe the voltage distribution inside the resonator. Full-wave simulations are used to evaluate the  $6 \times 6$  scattering matrix of a unit cell, based on the finite-element frequency-domain solver implemented in the CST Studio Suite by DS SIMULIA.

The short circuit at the end of the stub is made of a conductor with the same width as that of the microstrip stub and with a length of 0.56 mm, as shown in Fig. 1(a).

As explained earlier, the scattering matrix is then transformed into a  $6 \times 6$  transfer matrix of a unit cell. The voltage distributions at the various circuit nodes are calculated by cascading the transfer matrices of the unit cells.

In Fig. 2(b), the frequency response of the voltage at the middle of the finite structure with eight unit cells is plotted, where a peak is observed for each of the three microstrip lines at a resonance frequency close to the 6DBE frequency, i.e., at  $f_{r,6DBE} = 2.988$  GHz. Figure 2(c) shows the voltage distribution inside the eight-cell resonator at

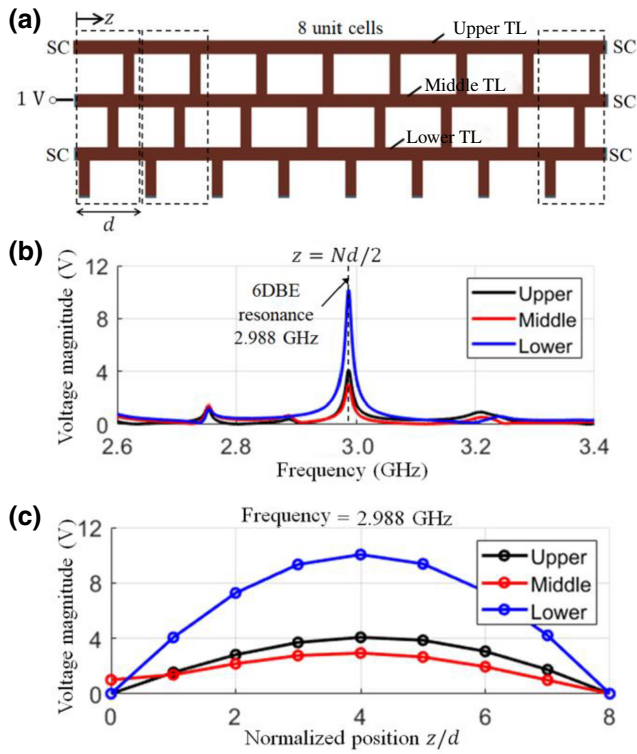


FIG. 2. (a) Resonance cavity formed by cascading eight unit cells (dielectric and underlying ground plane are not shown). All left and right terminations are shorted to the ground, except for the middle line at the left. We apply a phasor voltage of 1 V as the input to the resonator. (b) Frequency response of the voltage at the middle of the cavity; resonance peak is observed at a frequency close to the 6DBE frequency. (c) Voltage profile across the cavity at its 6DBE resonance frequency, showing the voltage distribution at each period of the three TLs. Upper, middle, and lower refer to TLs as shown in (a). SC in the figure refers to short circuit.

$f = f_{r,6DBE}$ , and we see that the voltage is concentrated around the middle of the structure, in particular, in the lower TL, as shown in Fig. 2(a), with the highest magnitude. This unique voltage distribution implies that anything connected, like a loading resistor, at the edges of the periodic waveguide will have a minor effect on the rest of the structure. The energy distribution in a 6DBE cavity is analogous to that obtained in resonators with second- or fourth-order DBEs [29]. This physical property is useful for conceiving alternative regimes of oscillation [30], and the voltage distribution provides information about where an active device can be placed to have the most significant impact [27]. It also demonstrates the “slow-light” effect associated with the DBE, where energy is trapped inside the cavity at a frequency near  $f_d$  [29].

The experimental verification of the existence of the sixth-order EPD in the microstrip three-way waveguide shown in Fig. 1(a) is presented. We use a grounded dielectric substrate (Rogers RO3003) and conductors like that

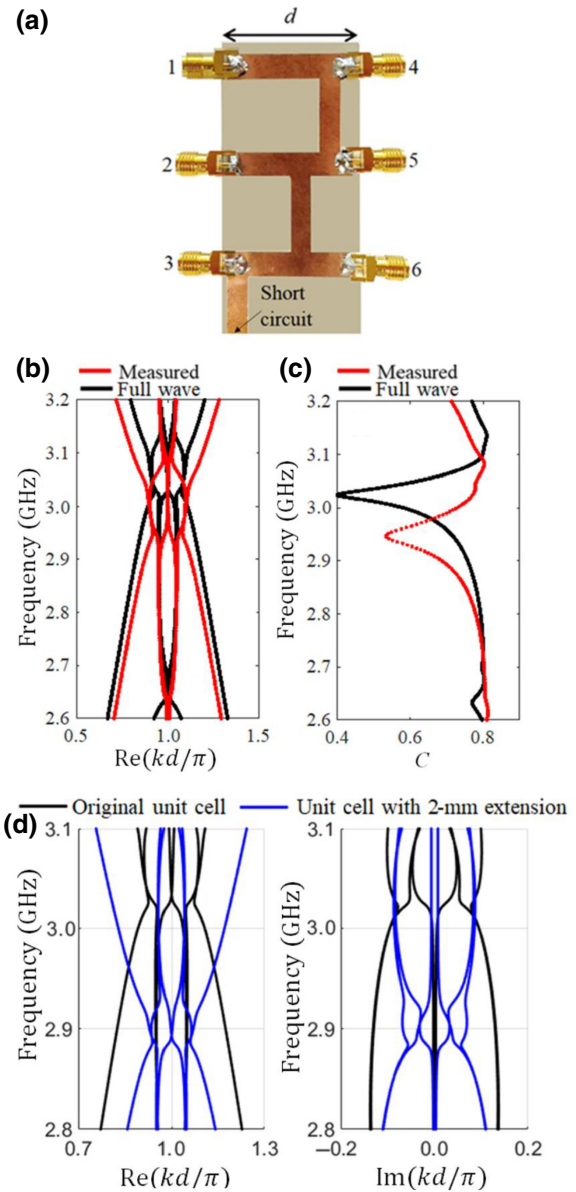


FIG. 3. (a) Fabricated unit cell of the proposed periodic three-way waveguide implemented in microstrip technology [ground plane is below the dielectric substrate (light brown)]. (b) Bloch-wave-number dispersion based on measurement (red dots) versus that obtained via method of moments full-wave electromagnetic simulation (solid black). Both measurement and simulation are based on a six-port evaluation of the scattering parameters of the unit cell. Six modes coalescing are clearly visible, although the coalescence is not perfect because of losses and manufacturing imperfections. (c) Coalescence factor,  $C$ , on linear scale versus frequency around the 6DBE, as a measure of closeness to the 6DBE, for the full-wave simulation results, in comparison to the measured results. (d) Tunability of 6DBE, showing dispersion diagrams obtained from full-wave simulation of the unit cell in Fig. 1(a) (black), and the same unit cell after adding 1-mm extension of the transmission line at each port (period is extended by 2 mm). Comparison shows that 6DBE frequency is very sensitive to any added extra length.

used for the full-wave simulations. The fabricated unit cell is shown in Fig. 3(a), including subminiature version A (SMA) connectors. The dispersion diagram obtained from the measurement of the  $6 \times 6$   $S$ -parameter matrix, along with the full-wave simulation results, are shown in Fig. 3(b). They are in a good agreement, although a shift in frequency is observed due to fabrication imperfections (especially knowing the exact line lengths) and high sensitivity of the sixth-order degeneracy to perturbations. The dispersion diagram shows the coalescence of the six modes based on measurements at the degeneracy frequency,  $f_d = \omega_d / (2\pi) = 2.95$  GHz. The measurement results are obtained by measuring the scattering parameters of the unit cell shown in Fig. 3(a) using a Rohde & Schwarz ZVA67 vector network analyzer (VNA).

The  $6 \times 6$   $S$ -parameter matrix is acquired by only using two ports of the VNA at a time, as illustrated in the following way. Port 1 of the VNA is connected to port  $m$  of the unit cell; port 2 of the VNA is connected to port  $n$  of the unit cell, while the four other ports are terminated by a  $50\text{-}\Omega$  load to measure  $S(m,n)$  [as well as  $S(n,m)$ ]. The obtained  $S$  parameters are smoothed out over frequency using MATLAB to eliminate the effect of random noise. Once the  $6 \times 6$   $S$ -parameter matrix is constructed, we obtain the  $6 \times 6$  transfer matrix,  $\underline{\mathbf{T}}$ , from which the Bloch wave numbers are solved for (as described previously). The wave numbers for both the measured and simulated results are plotted versus frequency to obtain the dispersion diagram shown in Fig. 3(b). These results show some perturbation and deviation from the ideal degeneracy condition (flat dispersion diagram at 6DBE frequency) in Fig. 1(b). The perturbation is due to the ohmic, dielectric, and radiation losses of the waveguide and to tolerances in fabrication.

Since an EPD is very sensitive to perturbations, we use a figure of merit to describe “how far” we are from an ideal EPD, based on the concept of the *coalescence parameter* or *hyperdistance*,  $C(\omega)$ , between the six eigenvectors of the transfer matrix of one-unit cell,  $\underline{\mathbf{T}}$ , as defined in Ref. [9]. The matrix is obtained here via measurements and full-wave simulations. The coalescence parameter presented in Eq. (3) is a very convenient figure to assess if an EPD occurs in reality, when losses and other perturbations are present. The perfect 6DBE that exists only mathematically would provide  $C=0$ . However, a system can still preserve the full-degeneracy properties when the eigenvectors are very close to each other, i.e., in the neighborhood of the 6DBE. The coalescence factor,  $C$ , is plotted in Fig. 3(c) as a function of frequency, accounting for all dissipative and radiative losses, showing good agreement between the two results based on measurements and full-wave simulations, in addition to a frequency shift. It can be seen that  $C$  has a minimum value in the vicinity of the 6DBE frequency ( $f = f_d$ ), as expected. In an

ideal lossless case, it is expected that  $C \rightarrow 0$  at the exact EPD.

The occurrence of the 6DBE implies that the system matrix is nondiagonalizable because the system has six repeated eigenvalues and one eigenvector,  $\Psi_e$ . This implies that the geometric multiplicity of the degenerate eigenvalue is equal to 1, while its algebraic multiplicity is equal to 6; hence, the transfer matrix,  $\underline{\mathbf{T}}$ , is not diagonalizable, and it is similar to a Jordan matrix,  $\underline{\mathbf{A}}_J$ , of  $6 \times 6$  dimension, with diagonal elements equal to  $\zeta_e = e^{-jked}$ . The matrix  $\underline{\mathbf{T}}$  can be represented as  $\underline{\mathbf{T}} = \underline{\mathbf{V}}\underline{\mathbf{A}}_J\underline{\mathbf{V}}^{-1}$ , where the similarity transformation matrix,  $\underline{\mathbf{V}}$ , is composed of one degenerate eigenvector and five generalized eigenvectors, which are associated with the eigenvalue,  $\zeta_e$ .

In practice, due to fabrication tolerances and losses of the structure, the system cannot operate exactly at the 6DBE but rather very close to it. When the system is close to the EPD, the system matrix is very close to being in a Jordan-block form. In this case, one can measure how close the system matrix is to the Jordan block through measuring how the eigenvectors of the system are close to each other using the previously mentioned concept of the coalescence parameter, as shown in Fig. 3. It is important to point out that the shift in the 6DBE frequency in the dispersion diagrams obtained from the measurements and full-wave simulation is mainly due to the extra lengths accounted for in the SMA connectors. De-embedding techniques, similar to those in Refs. [20, 31], can be applied to remove the effect of the SMA connectors on the measurements. Notably, the dispersion obtained from the measurement shown in Fig. 3(b) preserves the shape of the 6DBE, although de-embedding is not performed, and this shows that some tolerances can be fully accepted in the design. We confirm that the frequency shift is mainly due to the described effect by performing another full-wave simulation for the unit cell shown in Fig. 1(a), by using a similar unit cell with 1-mm extension of the TL at each port (hence, the unit-cell period is extended by 2 mm). We show in Fig. 3(d) a comparison between the two dispersion diagrams, which shows that the length extension does not impact the occurrence of the 6DBE but rather shifts its frequency. Therefore, we conclude that the extra lengths of the SMA connectors might lower the frequency at which the 6DBE occurs, as observed in Fig. 3(b). This result also shows a possible way to tune the 6DBE frequency.

In conclusion, a physical realization of a three-way periodic waveguide exhibiting sixth-order degeneracy (6DBE) is demonstrated using microstrip technology. The 6DBE is an exceptional point of sixth order where six eigenstates coalesce into a single degenerate one. Both theoretical and experimental verifications are provided. Remarkable physical properties may arise due to this

strong sixth-order exceptional point of degeneracy, including an increased quality factor, a high density of states, and improved sensitivity, which can lead to alternative designs for microwave and optical pulse generation [24], microwave and millimeter-wave oscillators [27,28,30,32], low-threshold lasers [22,33], short delay lines with significant group delay, filters, and ultrasensitive sensors. The fabrication and experimental demonstration of a DBE oscillator in microstrip technology was shown in Ref. [10], exhibiting very robust oscillation behavior. The 6DBE may lead to analogous or even superior performance, and it should be further investigated.

### ACKNOWLEDGMENTS

This material is based upon work supported by the National Science Foundation under Grant No. NSF ECCS-1711975 and by the Air Force Office of Scientific Research under Grant No. FA9550-15-1-0280.

- 
- [1] M. I. Vishik and L. A. Lyusternik, The solution of some perturbation problems for matrices and selfadjoint or non-selfadjoint differential equations I, *Russ. Math. Surv.* **15**, 1 (1960).
- [2] P. Lancaster, On eigenvalues of matrices dependent on a parameter, *Numer. Math.* **6**, 377 (1964).
- [3] T. Kato, *Perturbation Theory for Linear Operators* (Springer-Verlag New York Inc., New York, 1966).
- [4] A. P. Seyranian, Sensitivity analysis of multiple eigenvalues, *J. Struct. Mech.* **21**, 261 (1993).
- [5] A. Figotin and I. Vitebskiy, Frozen light in photonic crystals with degenerate band edge, *Phys. Rev. E* **74**, 066613 (2006).
- [6] A. Figotin and I. Vitebskiy, Slow wave phenomena in photonic crystals, *Laser Photonics Rev.* **5**, 201 (2011).
- [7] M. A. Othman and F. Capolino, Demonstration of a degenerate band edge in periodically-loaded circular waveguides, *IEEE Microw. Wirel. Compon. Lett.* **25**, 700 (2015).
- [8] M. A. Othman, F. Yazdi, A. Figotin, and F. Capolino, Giant gain enhancement in photonic crystals with a degenerate band edge, *Phys. Rev. B* **93**, 024301 (2016).
- [9] A. F. Abdelshafy, M. A. K. Othman, D. Oshmarin, A. T. Almutawa, and F. Capolino, Exceptional points of degeneracy in periodic coupled waveguides and the interplay of gain and radiation loss: Theoretical and experimental demonstration, *IEEE Trans. Antennas Propag.* **67**, 6909 (2019).
- [10] D. Oshmarin, A. F. Abdelshafy, A. Nikzamir, M. M. Green, and F. Capolino, Experimental demonstration of a new oscillator concept based on degenerate band edge in microstrip circuit, *ArXiv210907002 Phys* (2021).
- [11] C. Locker, K. Sertel, and J. L. Volakis, Emulation of propagation in layered anisotropic media with equivalent coupled microstrip lines, *IEEE Microw. Wirel. Compon. Lett.* **16**, 642 (2006).
- [12] J. L. Volakis and K. Sertel, Narrowband and wideband metamaterial antennas based on degenerate band edge and magnetic photonic crystals, *Proc. IEEE* **99**, 1732 (2011).
- [13] N. Gutman, C. Martijn de Sterke, A. A. Sukhorukov, and L. C. Botten, Slow and frozen light in optical waveguides with multiple gratings: Degenerate band edges and stationary inflection points, *Phys. Rev. A* **85**, 033804 (2012).
- [14] M. G. Wood, J. R. Burr, and R. M. Reano, Degenerate band edge resonances in periodic silicon ridge waveguides, *Opt. Lett.* **40**, 2493 (2015).
- [15] M. Y. Nada, M. A. K. Othman, and F. Capolino, Theory of coupled resonator optical waveguides exhibiting high-order exceptional points of degeneracy, *Phys. Rev. B* **96**, 184304 (2017).
- [16] T. Mealy and F. Capolino, General conditions to realize exceptional points of degeneracy in two uniform coupled transmission lines, *IEEE Trans. Microw. Theory Tech.* **68**, 3342 (2020).
- [17] M. A. K. Othman, X. Pan, G. Atmatzakis, C. G. Christodoulou, and F. Capolino, Experimental demonstration of degenerate band edge in metallic periodically loaded circular waveguide, *IEEE Trans. Microw. Theory Tech.* **65**, 4037 (2017).
- [18] A. A. Chabanov, Strongly resonant transmission of electromagnetic radiation in periodic anisotropic layered media, *Phys. Rev. A* **77**, 033811 (2008).
- [19] G. Mumcu, K. Sertel, and J. L. Volakis, Lumped circuit models for degenerate band edge and magnetic photonic crystals, *IEEE Microw. Wirel. Compon. Lett.* **20**, 4 (2010).
- [20] M. Y. Nada, T. Mealy, and F. Capolino, Frozen mode in three-way periodic microstrip coupled waveguide, *IEEE Microw. Wirel. Compon. Lett.* **31**, 229 (2021).
- [21] J. T. Sloan, M. A. K. Othman, and F. Capolino, Theory of double ladder lumped circuits with degenerate band edge, *IEEE Trans. Circuits Syst. Regul. Pap.* **65**, 3 (2018).
- [22] M. Y. Nada and F. Capolino, Exceptional point of sixth-order degeneracy in a modified coupled-resonator optical waveguide, *JOSA B* **37**, 2319 (2020).
- [23] M. A. Othman, V. A. Tamma, and F. Capolino, Theory and new amplification regime in periodic multimodal slow wave structures with degeneracy interacting with an electron beam, *IEEE Trans. Plasma Sci.* **44**, 594 (2016).
- [24] V. A. Tamma, A. Figotin, and F. Capolino, Concept for pulse compression device using structured spatial energy distribution, *IEEE Trans. Microw. Theory Tech.* **64**, 742 (2016).
- [25] C. R. Paul, *Analysis of Multiconductor Transmission Lines*, 2nd ed. (Wiley-IEEE Press, New York, 2007).
- [26] N. Dunford, J. T. Schwartz, W. G. Bade, and R. G. Bartle, *Linear Operators* (Wiley-Interscience, New York, 1971).
- [27] D. Oshmarin, F. Yazdi, M. A. K. Othman, J. Sloan, M. Radfar, M. M. Green, and F. Capolino, New oscillator concept based on band edge degeneracy in lumped double-ladder circuits, *IET Circuits Devices Syst.* **13**, 950 (2019).
- [28] M. Y. Nada, H. Kazemi, A. F. Abdelshafy, F. Yazdi, D. Oshmarin, T. Mealy, A. Figotin, and F. Capolino, in *2018 18th Mediterranean Microwave Symposium (MMS)* (2018), p. 108.
- [29] A. Figotin and I. Vitebskiy, Slow light in photonic crystals, *Waves Random Complex Media* **16**, 293 (2006).

- [30] A. F. Abdelshafy, D. Oshmarin, M. A. K. Othman, M. M. Green, and F. Capolino, Distributed degenerate band edge oscillator, *IEEE Trans. Antennas Propag.* **69**, 1821 (2021).
- [31] N. Apaydin, L. Zhang, K. Sertel, and J. L. Volakis, Experimental validation of frozen modes guided on printed coupled transmission lines, *IEEE Trans. Microw. Theory Tech.* **60**, 1513 (2012).
- [32] M. Radfar, D. Oshmarin, M. A. K. Othman, M. M. Green, and F. Capolino, Low phase noise oscillator design using degenerate band edge ladder architectures, *IEEE Trans. Circuits Syst. II Express Briefs* **69**, 1 (2021).
- [33] M. Veysi, M. A. K. Othman, A. Figotin, and F. Capolino, Degenerate band edge laser, *Phys. Rev. B* **97**, 195107 (2018).